Decisions on the fly in cellular sensory systems

Eric D. Siggia[a,1] and Massimo Vergassola[a,b,c,1]

[a]Center for Studies in Physics and Biology, The Rockefeller University, New York, NY 10065; [b]Physics of Biological Systems, Institut Pasteur, 75724 Paris Cedex 15, France; and [c]Centre National de la Recherche Scientifique, Unité Mixte de Recherche 3525, 75015 Paris, France

Contributed by Eric D. Siggia, July 29, 2013 (sent for review June 13, 2013)

Cells send and receive signals through pathways that have been defined in great detail biochemically, and it is often presumed that the signals convey only level information. Cell signaling in the presence of noise is extensively studied but only rarely is the speed required to make a decision considered. However, in the immune system, rapidly developing embryos, and cellular response to stress, fast and accurate actions are required. Statistical theory under the rubric of "exploit–explore" quantifies trade-offs between decision speed and accuracy and supplies rigorous performance bounds and algorithms that realize them. We show that common protein phosphorylation networks can implement optimal decision theory algorithms and speculate that the ubiquitous chemical modifications to receptors during signaling actually perform analog computations. We quantify performance trade-offs when the cellular system has incomplete knowledge of the data model. For the problem of sensing the time when the composition of a ligand mixture changes, we find a nonanalytic dependence on relative concentrations and specify the number of parameters needed for near-optimal performance and how to adjust them. The algorithms specify the minimal computation that has to take place on a single receptor before the information is pooled across the cell.

signal transduction | sequential probability ratio test

The exigencies of operations research during the second world war led to the following problem: Given a stream of data that is drawn from one of two prescribed models M1 or M2, what is the quickest way to decide between them subject to bounds on the errors? The solution found by Wald (1, 2) computes the ratio of two conditional probabilities using the data up to time t,

$$R(t) = P(\text{data}|M1)/P(\text{data}|M2), \quad [1]$$

and calls M1 when $R > H1$ and M2 when $R < H2$ and waits for more data otherwise. The thresholds H control the errors; e.g., larger $H1$ decreases the odds of deciding M1 when the data come from M2. For the task of distinguishing two Gaussians with different means, the average decision time for Wald's algorithm is a factor two times shorter than using a fixed averaging time for the same error rate. This is a simple example of a general class of problems termed "exploit–explore"; i.e., either decide or accumulate more data (3, 4). They are used in medical statistics to decide when a clinical trial has generated enough data for a conclusion.

For the problems that concern us, the next step in complexity was taken by Shiryaev (5–7), who considered the optimal detection of change points. A stream of data is presented and the model changes from M1 to M2 at an unknown time θ. The algorithm calls the change point at time t to minimize a linear combination of the false positive rate (e.g., $t \leq \theta$) and the decision time mean $(t - \theta)$ when $t > \theta$. Again the algorithm "knows" the models M1, M2.

Another step in complexity, about which we have little to say, corresponds to situations where the statistics of the hypotheses to be discriminated are not available or too elaborate to be exploited. An example in case is when the statistics of the stream of data are actively modified by the actions of the receiver; i.e., the decision process feeds back onto the input statistics. Optimal strategies are then difficult to prove but the "infotaxis" heuristic may apply in very uncertain situations, e.g., for biological problems such as searching for a source of molecules dispersed in a turbulent environment (8).

Neurobiology presents many examples of optimal decision problems as suggested by the title of a recent review, "Seeing at a glance, smelling in a whiff: Rapid forms of perceptual decision making" (9). These problems are amenable to experiment, typically posed in the Wald limit, and there are quantitative bounds on performance that are independent of neural parameters (10). The appeal is similar to that of investigating the performance of the eye, subject to the physical constraints of optics. However, when moving from mathematics to neural systems even theoretically, additional questions arise, such as, How well can neural circuits compute the optimal algorithm? How much memory is required? And is there some neuron whose firing level encodes the likelihood ratio R (11)?

In contrast to the extensive neurobiology and psychology literature, optimal decision theory has largely been neglected at the level of cell signaling, with the exceptions of refs. 12 and 13, in contrast to information theory that readily passes between the two domains (14–16). Rapid and accurate decisions seem as much a part of the cellular world as of the neural one. T cells in the immune system have to sample many protein fragments for potential antigens (17). Greater speed at fixed accuracy allows more extensive sampling. Bacteria have to sense DNA damage and respond appropriately (18). Chemotaxis by bacteria or eukaryotic cells such as neutrophils clearly is facilitated by rapid detection of gradients (19, 20). There is a plausible fitness gain if embryonic development is accelerated in species such as insects and amphibians that develop outside of the mother.

However, the signaling context requires different models than in neural systems. A natural model for a receptor, the signal transduction layer in neural terms, assumes that only the ligand binding times are available for downstream decisions. We show how simple analog computation built from standard biochemical

Significance

Cell-signaling pathways are often presumed to convert just the level of an external stimulus to response. However, in contexts such as the immune system or rapidly developing embryos, cells plausibly have to make rapid decisions based on limited information. Statistical theory defines absolute bounds on the minimum average observation time necessary for decisions subject to a defined error rate. We show that common genetic circuits have the potential to approach the theoretical optimal performance. They operate by accumulating a single chemical species and then applying a threshold. The circuit parameters required for optimal performance can be learned by a simple hill-climbing search. The complex but reversible protein modifications that accompany signaling thus have the potential to perform analog computations.

Author contributions: E.D.S. and M.V. designed research, performed research, contributed new reagents/analytic tools, analyzed data, and wrote the paper.

The authors declare no conflict of interest.

[1]To whom correspondence may be addressed. E-mail: siggiae@rockefeller.edu or massimo@pasteur.fr.

This article contains supporting information online at www.pnas.org/lookup/suppl/doi:10.1073/pnas.1314081110/-/DCSupplemental.

components can come close to the optimal performance. We consider both the fixed-time origin (Wald) and change-point problems. In each case we pose two computational tasks: sensing the absolute level of a single protein and detecting when the composition of a mixture changes at fixed total concentration. The uncorrelated nature of protein binding events implies that the accumulation of a single decision variable suffices for optimal performance, and no additional memory is needed. Parameter selection for the circuit doing the discrimination is clearly essential for optimal performance. Thus, we address the number of parameters needed for a good approximation and a plausible mechanism for their selection in vivo. In the embryo it may be reasonable to assume evolution has jointly optimized the signal and receiver to ensure rapid information transmission.

The statistical theory of Wald and his successors is predicated on the assumption that the data presented to the decision machinery are derived from one of the two models being compared. Mathematics furnishes no guidance as to how Eq. **1** performs otherwise. We show by example that counter to intuition, when the data are "easier", i.e., present a greater contrast than the model assumes, the performance of Eq. **1** can actually degrade. This problem can be "cured" by suitably generalizing the states being compared. This complicates the calculations, but is required for biological realism.

Results

The typical vertebrate signaling pathway has over 10 genes that operate from the presentation of a signal to its realization through transcription (www.stanford.edu/group/nusselab/cgi-bin/wnt/; refs. 21, 22). This complexity seems in excess of what is needed to transmit merely level information and the component overload is attributed to the exigencies of biochemistry or evolutionary accident. We consider the alternative that natural signals are dynamic and the pathway uses that temporal history to make decisions. Because there are few single-cell experiments that present complex signals, we suggest some problems the cell may need to solve and compute the performance of simple biochemical systems.

We assume that the only information a single receptor has about the extracellular environment is whether it is bound by a ligand or not. Binding can of course elicit downstream changes in receptor conformation, binding to other receptors, and phosphorylation cascades, all of which we consider as possible analog "computations" performed on the time history of receptor occupancy. We consider two idealized tasks: (*a*) distinguishing two concentrations of the same ligand and (*b*) detecting a new component (or agonist in the immune context) added to a preexisting "pure" or "self" state. We keep total concentration fixed when the composition changes in *b* to distinguish the problem from *a*. The temporal context can be either (*i*) data from one of the possible states are presented at a defined time $t = 0$ or (*ii*) the data change from state *i* to state *ii* at an unknown time that is to be determined. For all combinations of tasks and contexts, the cell has to decide as rapidly as possible subject to an error bound. We first pose our two computational tasks (*a*, *b*) in the Wald limit with a defined initial time, i.e., a ratio test, Eq. **1**, and then consider the more realistic (time) change-point problem.

Ratio Test for Concentrations. Consider a single receptor that is empty/occupied for a series of times $[s_1, t_1, s_2, t_2, ..]$; then the probability for observing the corresponding transitions is

$$P(s_i, t_i) = ke^{-ks_1}ds_1\nu e^{-\nu t_1}dt_1 ke^{-ks_2}ds_2\cdots, \qquad [2]$$

where k is the on rate and ν is the off rate and the string of events is cut off by the current time t. Because we are interested in the long time limit, we do not consider the initial state and assume t falls just after one of the s_i, t_i. With only one species of ligand, the Wald sequential probability ratio test (SPRT) takes the ratio of Eq. **2**, evaluated for the two concentrations under consideration. Then the factors $\nu e^{-\nu t_i}$ cancel because the dissociation events do not distinguish between the hypotheses; the off rates are identical. Setting $k = \phi L$ for the two ligand concentrations $L_{1,2}$, one finds

$$\ln\left(\frac{P(L_2)}{P(L_1)}\right) = -\phi(L_2 - L_1)\int_0^t (1 - n(s))ds + J_+(t)\ln\left(\frac{L_2}{L_1}\right), \qquad [3]$$

where $n(t) = 0, 1$ is the receptor occupancy at time t and $J_+(t)$ is the number of 0→1 transitions up to t.

For times much longer than the typical binding/unbinding times, we expect that the log-likelihood ratio is well approximated by Gaussian diffusion with drift. In *SI Appendix*, we detail the calculation of the receptor occupancy statistics that allows us to obtain the mean and the diffusivity for the log-likelihood. The expression for the drift reads

$$\frac{d}{dt}\left\langle \ln\left(\frac{P(L_2)}{P(L_1)}\right)\right\rangle = \frac{\nu\phi}{\nu + \phi L}\left[L_1 - L_2 + L\ln\left(\frac{L_2}{L_1}\right)\right]. \qquad [4]$$

The concentration L corresponds to the real process generating the data, which can possibly differ from the concentrations assumed in computing the probability ratio, Eq. **3**. Note that the drift, Eq. **4**, is defined as the rate of information production since the left-hand side (for data generated by one of the two models) is the rate of increase of the Kullback–Leibler relative entropy between the two distributions to be discriminated, which controls the error in hypotheses discrimination (Chernoff–Stein lemma; see, e.g., p. 383 in ref. 23).

It is important to consider the behavior of the average drift, Eq. **4**, when the data presented to the ratio test, represented by L, do not correspond to either of the two ligand concentrations, $L_{1,2}$ assumed in constructing the ratio. For $L_1 > L_2$ the drift is a monotone decreasing function of L. Thus, if $L > L_1$ or $L_2 > L$, i.e., the data are easier to discriminate than the model assumes, the average drift will move the probability ratio more rapidly toward the decision thresholds. (The analogous remarks hold if $L_1 < L_2$.) More formally, if one desires to distinguish two states of concentration that can lie above or below a band around $\overline{L}$, then the strategy that ensures that the most difficult case is done as well as possible (Maxi-Min strategy in game theory) would be to chose $L_{1,2}$ in Eq. **4**, as the concentrations defining the excluded band.

The diffusion approximation to the SPRT log-likelihood maps the decision process into the first passage time for two adsorbing boundaries and permits the analytic calculation of the decision time in terms of the imposed error rates (*SI Appendix*). The diffusion approximation works well provided the decision is based on several binding/unbinding events, as shown in Fig. 1. An important consequence of the analytical formula that we derive in *SI Appendix* is that the average decision time behaves as $1/(L_1 - L_2)^2$ for small differences between the two levels to be discriminated. It follows that the discrimination of a 1% difference requires times of the order of 10^4 (in units set by the timescale of the elementary events) (Fig. 1).

The scaling of the inverse decision time with the square of the concentration difference is just a restatement of the law of large numbers and was first used in chemo-sensory context by Berg and Purcell (24) and refined as a maximum-likelihood calculation in ref. 25. The question being addressed in these papers is: How accurately can the concentration be measured from binding events occurring over a prescribed length of time? The SPRT asks a different question and although the scaling with concentration is the same, the average decision time must be faster and Fig. 1 shows a speedup by two to three times for the same error rate. Although the maximum-likelihood calculation is of course

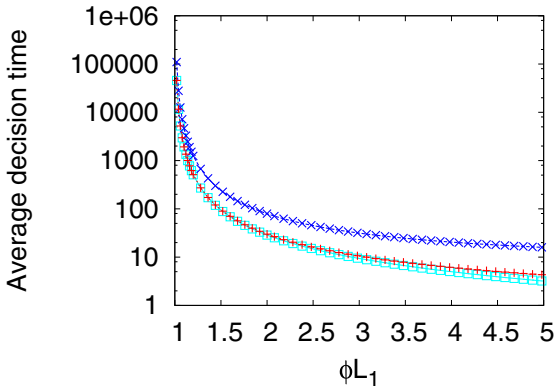

Fig. 1. Average decision time for the Wald SPRT (red +) and its diffusion analytical approximation (aqua squares) derived in *SI Appendix*. The model parameters are $\nu = 1$, $\phi L_2 = 1$, with variable ϕL_1 on the abscissas. The data for discrimination are sampled with an on rate $\phi L = 1$. Precisions (false positive and false negative fractions) are 1%. The blue Xs are the times that would be required by standard maximum-likelihood decisions, using a fixed sample size, the length of which is chosen to ensure the same 1% precision (see *SI Appendix* for details). Note that Wald's SPRT is more than twofold faster than standard maximum likelihood even in the asymptotic regime of small $L_1 - L_2$.

a valid bound, if one thinks mechanistically about a gene network, it is more likely that a "decision" is made when sufficient information accrues, rather than after a prescribed averaging time encoded in the genome. Note also that the distribution of completion times for a gene network, such as one would compute by Laplace transforming the master equation, is logically distinct from the SPRT that gives the optimal bound for the average decision time for any algorithm.

Ratio Test for Mixtures. Consider a situation where a ligand with off rate ν_1 is presented to the receptor alone or mixed with a second ligand with off rate $\nu_2 < \nu_1$. We assume the on rates per molecule are the same and the total concentration is invariant so now only the off rates survive when the ratio of Eq. **2** is formed. The analog to Eq. **3** is constructed by taking the ratio of the probability per time for a jump off the receptor under the mixture assumption, $(1-w)\nu_1 e^{-\nu_1 t} + w\nu_2 e^{-\nu_2 t}$, to the same quantity with $w = 0$, which is the probability density in the pure ensemble,

$$R(w,t_i) = 1 - w + w\frac{\nu_2}{\nu_1}e^{(\nu_1-\nu_2)t_i}, \qquad [5]$$

$$\ln\left(\frac{P(w)}{P(0)}\right) = \sum_{i=1}^{n} \ln R(w,t_i), \qquad [6]$$

where $w \ll 1$ is the fraction of the second ligand in the mixture, t_i are the binding times, and the sum on n is constrained by the total time t. If the ligand is bound at the current time t, the last term in the sum is slightly different as it does not contain the factor ν_2/ν_1; we neglect here this minor correction to simplify notation (see *SI Appendix* for more details). Note that the optimal function to discriminate between the two hypotheses, pure vs. mixture, contains three parameters characterizing the data: $w, \nu_{1,2}$.

The immune system presents a typical example of the type of discrimination task we are studying. Thus, one interesting limit is $\nu_1/\nu_2 > 2$ and $w \ll 1$; there are a few agonists that bind to the T-cell receptors for more than twice as long as self. Then the leading terms in both the average and the variance of Eq. **5** (and thus the decision time) are nonanalytic in the admixture and scale as $w^{\frac{\nu_1}{\nu_1-\nu_2}}$. To be explicit, the sum over the independently sampled t_i in Eq. **6** converges to the integral of $\ln(R)$ in Eq. **5** over either the pure $(\rho(t_i) = \nu_1 e^{-\nu_1 t_i})$ or the mixture $(\rho(t_i) = w\nu_2 e^{-\nu_2 t_i} + (1-w)\nu_1 e^{-\nu_1 t_i})$ distributions. The leading, and singular term for small w can be derived explicitly by changing variables in the integral average over the distributions and agrees with the exact hypergeometric function in *SI Appendix*, Eqs. **24** and **25**,

$$\langle \ln R(w,t)\rangle_{pure} \simeq -\left(\frac{\nu_2}{\nu_1}\right)^{\alpha}\frac{w^{\alpha}}{\alpha-1}\int_0^{\infty}\frac{x^{1-\alpha}}{(1+x)^2}dx, \qquad [7]$$

$$\langle \ln R(w,t)\rangle_{mix} \simeq \left(\frac{\nu_2}{\nu_1}\right)^{\alpha}\frac{w^{\alpha}}{\alpha-1}\int_0^{\infty}\frac{x^{1-\alpha}}{1+x}dx, \qquad [8]$$

where $\alpha \equiv \frac{\nu_1}{(\nu_1-\nu_2)}$ and $1 < \alpha < 2$. Numerically Eqs. **7** and **8** are $\sim(0.7, 0.92)$ times the exact values for $w = (0.1, 0.01)$, respectively, and corrections scale as $O(w^2)$. For $1 < \nu_1/\nu_2 < 2$ all quantities scale as w^2 and Eqs. **7** and **8** do not apply.

The average decision time is shown in *SI Appendix* to be $\propto 1/\text{drift} \times f(\text{drift}/\text{variance})$, where f is a function computed explicitly and drift and variance refer to the log-likelihood of $\ln(R)$ in Eq. **5**. The formula is derived using the diffusion approximation, which is justified as decision times are very long in the limit $w \to 0$. Because the average and the variance of $\ln(R)$ in Eq. **5** have the same scaling in the limit of small w, we conclude that the decision time behaves as w^{-2} or $w^{-\alpha}$, depending on the ratio ν_1/ν_2.

The fractional power of w in the decision time for $\alpha < 2$ can be derived in elementary terms by posing a suitable statistical test. Given a total of N samples, define a cutoff time T such that $Ne^{-\nu_1 T} \sim 1$; i.e., we expect to see only one event longer than T in the pure ensemble. Then the minority constituent of the mixture is visible in the tail of the distribution if the expected number of LONG events for the mixture, $Nwe^{-\nu_2 T} \gg 1$. Eliminating T from the two equations gives $N \gg w^{-\alpha}$, which agrees with the exact calculation. It is obviously easier to detect a minority constituent with a longer rather than shorter off time than that of the host.

When $1 < \nu_1/\nu_2 < 2$, we can estimate how the decision time varies with w by comparing the difference in mean receptor occupancy times in the pure and mixed ensembles and comparing with the standard deviation (SD). That is, $w(1/\nu_2 - 1/\nu_1)$ exceeds the variance, $1/(\nu_1\sqrt{N})$, provided $N \gg \frac{1}{w^2}$. This agrees with the previous estimate when $\nu_1 = 2\nu_2$ and is less stringent, i.e., allows smaller N, when $\nu_1 < 2\nu_2$.

Now in analogy with the discussion of Eq. **4** when the data L differ from the concentrations $L_{1,2}$ assumed in the model, we inquire how the ratio test for mixtures performs when the off rate for the majority component of the data ν_d is larger than the analogous parameter, ν_1, in Eq. **5**. This should make it easier to detect when the minority species with a smaller off rate $\nu_2 < \nu_1 < \nu_d$ is present. However, for large enough ν_d the ratio test will classify the mixture data as pure (Fig. 2). The long binding events correctly favor the mixture, but the excess of short events contributes a negative drift to $\ln R(w,t)$ that eventually overwhelms the positive drift from the long events (*SI Appendix*, Fig. S4). To fix this problem we need to include a realistic formulation of the pure system, namely of the fact that it might be composed of several types of ligands and that its exact composition is generally unknown.

Assume the pure system consists of a mixture of M species with off rates ν_i and unknown weights w_i that sum to one. Then the probability of observing a string of times $t_i, i = 1, \ldots, N$ is computed from the probability of the times conditioned on the weights followed by an integral over the w_i with a prior we take as flat,

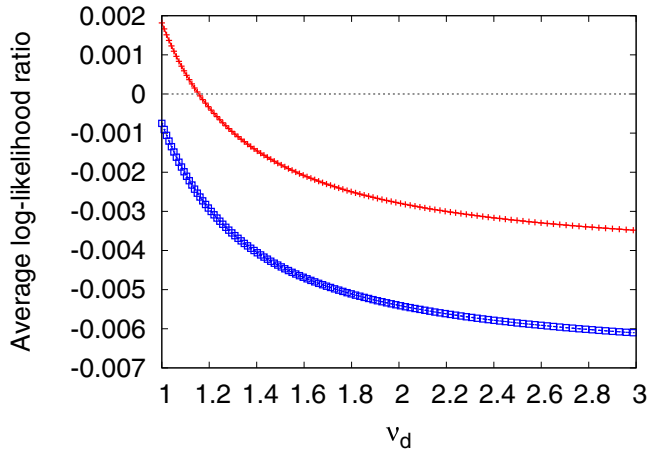

Fig. 2. The ratio test can fail when the data presented do not conform to the model. The average of the log-likelihood ratio as defined in Eqs. **5** and **6** is plotted vs. the off rate of the majority component in the data, ν_d. The model has $w = 0.01$, $\nu_1 = 1$, and $\nu_2 = 0.3$. The upper curve (crosses) refers to mixture data with the same w and off rates ν_d,ν_2 whereas the lower one (squares) refers to data generated entirely with the off rate ν_d. The upper curve is positive for $\nu_d \sim \nu_1$, but ultimately becomes negative, implying a failure to detect the mixture.

$$p(t|\boldsymbol{w}) = \sum_{i=1}^{M} w_i \nu_i e^{-\nu_i t}, \qquad [9]$$

$$P(t_1, \ldots, t_N) = \int d\boldsymbol{w}\delta\left(\sum_{i=1}^{M} w_i - 1\right) e^{\sum_{i=1}^{N} \ln(p(t_i|\boldsymbol{w}))}. \qquad [10]$$

For large N the integral over $\boldsymbol{w}$ can be evaluated by a saddle point. The sum over the t_i in the saddle equation for the w_i should self-average and can be replaced by the time ensemble average. It is easy to check that the saddle equation for w_i is always solved by the w_i used to generate the data if the ν_i of data and model are the same; otherwise the solution is nontrivial. The $\mathcal{O}(N)$ term from the saddle has calculable $\mathcal{O}(\log N)$ corrections from fluctuations around the saddle (*SI Appendix*). The choice of prior, provided it is smooth and nonzero around the saddle, contributes only a constant. The same calculation can be done for the mixture data, with of course an independent integral over the relevant weights and a new saddle point (*SI Appendix*).

Thus, the optimal decision method to distinguish the admixture of a minority of long-lifetime species in a soup of shorter residence times implicitly determines the composition of the soup. This would seem to make an analog biochemical calculation insurmountable. However, the existence of a saddle point approximation does imply that the optimal algorithm can estimate the ratio by two terms of the form in Eq. **9** with distinct and unknown values of $\boldsymbol{w}$. We develop below an approximation to Eq. **9** that can be easily optimized and biochemically implemented. Thus, optimizing the parameters in a biochemical model that locates the time change point will implicitly incorporate information about the saddle approximation, without requiring the intermediate solution of Eq. **10**. The existence of a saddle approximation suggests that optimization of the complete problem could be simple, and indeed it is, as shown below.

Change Point for Mixtures. We now shift from the problem of distinguishing two states presented at a defined time to finding the time when the state changes in a defined way. In the previous case where the statistics of the log probability ratio were Gaussian and easy to calculate with no further approximations, the change-point problem is more overtly dynamic.

Shiryaev (5, 6) considered the process $\dot{x} = \chi(t-\theta) + \eta$, where χ is the Heaviside step function, $\chi(t \le 0) = 0, \chi(t > 0) = 1$, η is δ-correlated noise, and the change-point θ has a Poisson distribution defined by its rate. The task is to define an algorithm to determine θ from a stream of data $x(t)$ that minimizes a linear combination of the false positive rate or precision and the decision time [average of $(t-\theta)\chi(t-\theta)$]. We assume θ is Poisson distributed, so ultimately the change happens, but one can equally formulate a stationary problem with a limit on the false positive rate per time (7).

As before the optimal solution computes the probability ratio that the change at time θ happens before the current time, normalized by the probability it has not yet happened, with all probabilities conditioned on the history of $x(t)$; symbolically, $Q(t) = P(t > \theta | x(0 \ldots t))/P(t < \theta | x(0 \ldots t))$. A decision is made when $Q \ge H$, where H is a numerical parameter related to the assumed error function. When x derives from white noise, Q can be computed incrementally in time with no auxiliary memory, and explicit expressions are given in *SI Appendix* for several cases.

We can again time slice the continuous-time recursion for Q after each off event n as was done in Eqs. **5** and **6**. The discrete iteration reads in the simplest case of only two off rates (see *SI Appendix* for details),

$$Q_n = \frac{R(w, t_n)}{1-\lambda}(\lambda + Q_{n-1}), \qquad [11]$$

where Q_n is the conditional probability ratio, just defined, after the series of the $t_1, \ldots, t_n$ unbinding events, $R(w, t_n)$ is the probability ratio defined in Eq. **5**, and λ is the probability per iteration for the change of statistics; i.e., $\lambda(1-\lambda)^{n-1}$ is the probability that the change point will occur for the nth binding event. To bridge the reduction of Eq. **11** to an analog computation and deal with extensions, e.g., Eqs. **9** and **10**, it is expedient to introduce the following iterative model for the mixture change-point problem that can be solved analytically and is derived by taking the log of Eq. **11**:

$$y_n = -c + \max(t_n - T, 0) + \max(y_{n-1}, 0). \qquad [12]$$

Its relation to Eq. **11** is apparent if we set $Q = \lambda e^y$, approximate $\ln(1 + e^y) \sim \max(y, 0)$ and $\ln(R) = \ln\left(1 - w + w\frac{\nu_2}{\nu_1}e^{(\nu_1-\nu_2)t}\right) \sim -c_1 + c_2\max(t-T, 0)$, and finally rescale both $c_1 + \ln(1-\lambda)$ and y to eliminate c_2. The true probability ratio directly translates to the error rate and the decision threshold, H, for Q_n in Eq. **11** is largely independent of the data. However, because of rescalings, the threshold for Eq. **12** is contingent on the data, as are c, T. The entire parameter space of the model is thus 3D (c, T, H). The piecewise linear approximation to Eq. **5** is accurate in mean square to $\sim 1\%$ for all $w < 0.2, \nu_2 < 0.3\nu_1$.

Eq. **12** makes it intuitive that the optimal decision algorithm takes either a small downward step of $c \sim w/(\nu_1 - \nu_2) \ll 1$ with probability $\sim 1 - e^{-\nu_1 T}$ or an occasional $\mathcal{O}(1)$ step upward. The floor on y encodes the prior expectation of a fixed probability per time for a change in data to occur. Clearly an accurate decision based on the criterion $y \ge H$ requires a positive drift $v_y \equiv \langle -c + \max(t-T, 0)\rangle_{mix}$ in the mixture ensemble and a near zero or negative drift $v_y \equiv \langle -c + \max(t-T, 0)\rangle_{pure}$ in the pure ensemble to avoid reaching the threshold before the switch of the statistics, i.e., typically $\simeq 1/\lambda$ iterations.

In the pure ensemble, y has a stationary distribution that can be calculated along with the rate per iteration, γ, that y hits H. The drift-diffusion approximation that we used for the probability ratio accumulated from a fixed time does not work for

Eq. **12** but we can use the so-called Poisson clumping heuristics (26) to obtain the corresponding error rate (see *SI Appendix* for details). We work in the limit $c \ll 1$ and lump all instances of $y < 0$ into $\delta(y)$,

$$\beta = \nu_1 - e^{-\nu_1 T}/c > 0, \quad [13]$$

$$\mathrm{PDF}(y) = \frac{\beta}{\nu_1}\delta(y) + \frac{\beta e^{-\nu_1 T}}{\nu_1 c} e^{-\beta y}, \quad [14]$$

$$\gamma = \frac{e^{-\beta H - \nu_1 T}}{\nu_1 c + \nu_1^2/\beta^2}. \quad [15]$$

The parameter γ is the intrinsic characterization of the false positive rate, i.e., per iteration of Eq. **12**. The false positive rate per trial used for Eq. **11** is recovered by multiplying γ by the expected waiting time, i.e., the average of θ or $1/\lambda$. Using Eq. **15**, the threshold H can be calculated from the false positive rate. To find the average decision time one can then initialize y by sampling from Eq. **14** to generate binding times from the mixture ensemble and iterate until hitting H.

We can now quantify the errors inherent in the Eq. **12** model by using the natural error metric of the average decision time at a fixed false positive rate. If we take data generated with the same parameters $\nu_1 = 1$ and $\nu_2 = 0.3$ as in Fig. 2, $\gamma \sim 10^{-5} - 10^{-4}$, and $w = 0.1$, then Eqs. **11** and **12** give decision times within 10% (Fig. 3). In fact, simulating Eq. **12** over a grid of (c, T) parameters shows a limited band where the drift velocity, v_y, has the appropriate sign for both the pure and the mixed data. The shape of the decision-time landscape in Fig. 4 shows that the optimum is easy to reach by any gradient-descent evolution. This observation is relevant for the biochemical implementation of Eq. **12** that is described below.

When multiple frequencies are included in the pure ensemble, the situation is as follows. If the weights of the various frequencies composing the data are known to the model, then Eq. **11** still applies with the probability ratio Eq. **5** replaced by

$$R'(w,t) = 1 - w + w\frac{\nu_a e^{-\nu_a t}}{\sum_{j=1}^{M} w_j \nu_j e^{-\nu_j t}}, \quad [16]$$

where the denominator coincides with the likelihood previously defined in Eq. **9** and ν_a is the frequency of the new molecular species (antigen) added into the mixture at a random time.

If the weights w_j in Eq. **16** are not a priori known, then Bayesian integrals as in Eq. **10** are required. When a new binding event t_{N+1} is added to the sum in the exponential of the integrand in Eq. **10**, the value of the resulting integral $P(t_1, \ldots, t_N, t_{N+1})$ is not obviously related to $P(t_1, \ldots, t_N)$ and t_{N+1} (except in the limit of large N when a saddle approximation is justified) (*SI Appendix*). Determining the Bayesian optimal decision becomes then quite involved even from a purely computational perspective, let alone implementing it biochemically.

However, as shown in Fig. 3, the three-parameter Eq. **12** model cuts this Gordian knot, ensuring sensible speed and accuracy. Comparing its performance to that of Eq. **11** for a random ensemble of mixtures, we see indeed that speed is slower by 20–30% only, over a broad range of precisions. It is worth remarking that in Eq. **16** we are using the information on the weights in the mixture for each realization of the data. We have checked on a few realizations that discarding this information and calculating the optimal decision with Bayesian integrals as in Eq. **10** yields, as expected, a decision-time intermediate between Eq. **11** and Eq. **12**.

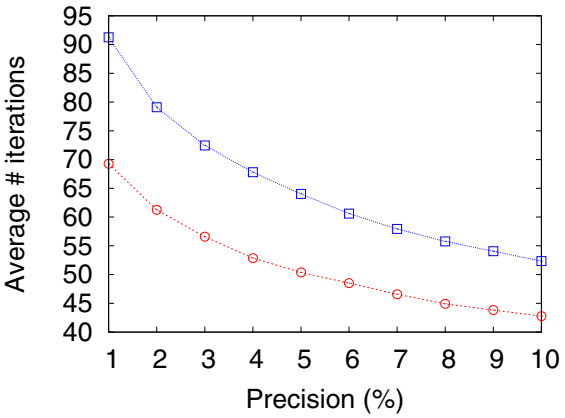

Fig. 3. Decision time for the optimal strategy, Eq. **11** (circles), compared with the three-parameter model, Eq. **12** (squares), for a range of precisions. (In addition, Eq. **11** uses the actual composition of the data.) The mixture is generated with three frequencies $\nu_1 = 1$, $\nu_2 = 1.5$, and $\nu_3 = 2$ and its composition is random. The agonist species with $\nu_a = 0.3$, $w = 0.1$ is added to the mixture at a Poisson-distributed time with mean $1/\lambda = 100$ in iteration units.

The histogram of decision times for both the ratio test and the change-point problems is contained in *SI Appendix*, Fig. S2. Both distributions have an exponential tail that is $\sim 1.5 - 1.6$ times narrower than a Poisson distribution, when normalized by the mean time.

Biochemical Networks to Implement the Ratio Test for Concentrations. We now show that the calculation of the log-likelihood ratio Eq. **3** can be realized with standard biochemical reactions. This is particularly simple because we just have to simulate by analog means an initial value problem: The ratio test presumes an origin of time, i.e., when the receptor is first exposed to ligands of either concentration.

A simple procedure that gives a good approximation is to have two chemical species E_1 and E_2. We assume $L_2 > L_1$ (the opposite case is treated similarly). The first enzyme decays exponentially when the receptor is unbound as $\frac{dE_1(t)}{dt} = -\phi(L_2 - L_1)E_1(t)$ whereas the second decays when the receptor is bound as $\frac{dE_2(t)}{dt} = -\alpha E_2(t)$, where α is a constant. The two species represent, respectively, the exponential of the first and the second term (with the sign inverted) in the expression Eq. **3**. The E_1 equation is exact, whereas the one for E_2 is just an approximation because the decay in Eq. **3** is proportional to the binding time and not fixed.

As for the choice for the constant α, when many binding events accumulate, the average binding time will be $1/\nu$. If we want to reproduce at least on average the correct result that upon binding there should be a factor L_2/L_1 in the likelihood ratio, then we should choose $\alpha = \nu \log(L_2/L_1)$. Validity of the choice is confirmed numerically in *SI Appendix*.

The next biochemical layer computes E_1/E_2, which approximates the likelihood ratio and switches when it reaches an appropriate threshold. A biochemical switch that produces such an output is the Goldbeter–Koshland module (27). The two species E_1 and E_2 act enzymatically in opposite directions on the conversion between two forms A and A^*. The detailed scheme is

$$A + E_1 \leftrightarrow AE_1 \rightarrow E_1 + A^*; A^* + E_2 \leftrightarrow A^*E_2 \rightarrow E_2 + A. \quad [17]$$

The association/dissociation rates in the bidirectional reactions are denoted a_1, d_1 and a_2, d_2, respectively. The two subsequent dissociation reactions proceed at rates k_1 and k_2. In the limit when the total amount of the two enzymes $E_{1T}, E_{2T} \ll A_T$, the

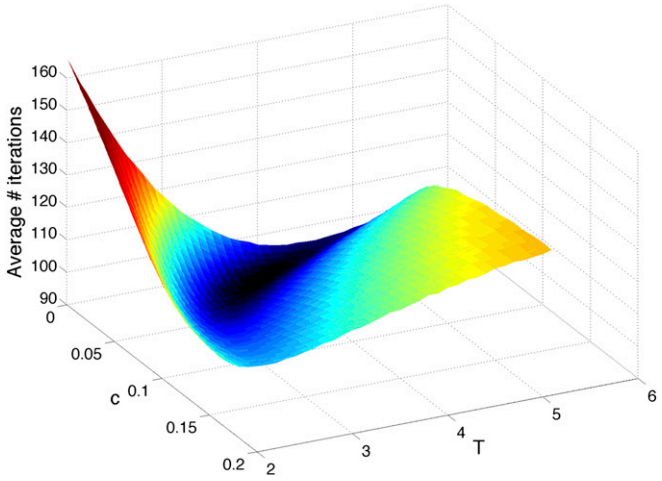

Fig. 4. The landscape of the average number of iterations required for decision vs. c,T for the Eq. **12** model. The precision of the decisions is 1% and averages are obtained over 10^7 realizations. The parabolic shape makes parameters easy to optimize by evolutionary gradient descent.

steady-state normalized concentrations $A = [A]/A_T$ and $A^* = [A^*]/A_T$ depend on the ratio E_{1T}/E_{2T} only,

$$\frac{E_{1T}}{E_{2T}} = \frac{k_2}{k_1}\frac{A^*(1-A^*+K_1)}{(1-A^*)(A^*+K_2)}, \qquad [18]$$

where $K_1 = (d_1+k_1)/(a_1A_T)$ and $K_2 = (d_2+k_2)/(a_2A_T)$. Inspection of **[18]** shows that for $K_1, K_2 \ll 1$, a sharp switch occurs around $k_1E_{1T} = k_2E_{2T}$ and the output A^* features a jump from values very small to close to unity. This is the regime that is of interest to us. We can then use two Goldbeter–Koshland modules with rates k_i adjusted so that they switch to signal a decision at the high or low threshold values of the probability (enzyme) ratio. The response time of the Goldbeter–Koshland (GK) system does slow down at the transition point, but this is not a serious issue for us, because either the forward or the backward rate is monotone increasing and thus moves through the transition region, and the decision becomes rapid. Our simulations of course include proper dynamics at the transition point in the GK system.

Results of numerical simulations for the previous model are shown in Fig. 5. The main source of error is due to the fact that E_2 decays at an average rate for the whole period of measurement rather than separately and discretely registering each binding as in Eq. **3**. The quality of the approximation can therefore be improved by assuming adaptation mechanisms for the receptors. In refs. 12 and 13 it was for example assumed that receptor inactivation is the most rapid time. We have verified that fast adaptation permits the system to approach the optimal behavior when measuring on rates but obviously sacrifices all sensitivity for off rates and thus is not a strategy we could use to detect a small admixture of agonist. It is also not clear for all classes of receptors that the requisite speed is molecularly achievable. We thus present data without any receptor adaptation to show that results are still very good and deviate by a factor two times that of optimal over a broad range of precisions.

An alternative to regulated decay that computes an exponential is autophosphorylation, analogous to simple noncooperative feedback of a transcriptional activator on itself. If receptors that dimerize and transactivate were able to rapidly exchange partners, then the number of activated receptors would grow exponentially. We are not aware whether this possibility has been considered experimentally.

Biochemical Networks to Detect a Mixture Change Point. A true ratio test, in the sense of the previous section, would occur in a cell if there was an initial signal to start the process and a second system that did the comparison as an initial value problem. More likely is a single receptor that continuously monitors the environment and needs to detect when the composition changes, i.e., the Shiryaev problem.

The near optimal computation of a change point with the model of Eq. **12** simplifies its realization in biochemical terms. Consider a typical system with slow on, fast off dynamics; e.g., the ligand-bound receptor complex has a sequence of phosphorylation states, $C_i, i = 0,\dots,N$. There is a forward rate ω for $C_i \to C_{i+1}$, a ligand unbinding rate ν, and a rapid reversion of any C_i to the unphosphorylated receptor when the ligand falls off. Only C_N can activate downstream events. If C_0 is initialized at 1, then $C_i(t) = \frac{(t\omega)^i}{i!}e^{-(\nu+\omega)t}, i = 0,\dots,N-1$ and $C_N = \int_0^t \omega C_{N-1}(t')e^{-\nu(t-t')}dt'$.

If instead we ask for the probability of C_N conditioned on the receptor being continuously bound for a time span t, then we can remove the unbinding event ν from the rate equations and find

$$P(C_N(t)|\text{bound}) = \int_0^t \frac{t'^{N-1}\omega^N}{(N-1)!}e^{-\omega t'}dt'. \qquad [19]$$

For large t, Eq. **19** tends to 1 as it should, and it is $\ll 1$ for $t < 1/\omega \sim T$. To reproduce $\max(t-T,0)$ in Eq. **12** it is then sufficient to let C_N act enzymatically on some substrate present in excess. The small constitutive negative drift in Eq. **12** could be replicated by an enzymatic degradation in a saturated regime (see ref. 28 for a biological instance of such a mechanism). In summary, the proposed chemical equivalent to Eq. **12** in differential form reads

$$\dot{z} = C_N(t) - c_1\frac{z}{z+\epsilon}. \qquad [20]$$

The positivity of y in Eq. **12** is naturally encoded by a concentration, z. The decision is made when z hits some value H and any scale factor multiplying C_N can be adsorbed into H. Provided $\epsilon \ll H$, precisely how the degradation saturates does not matter,

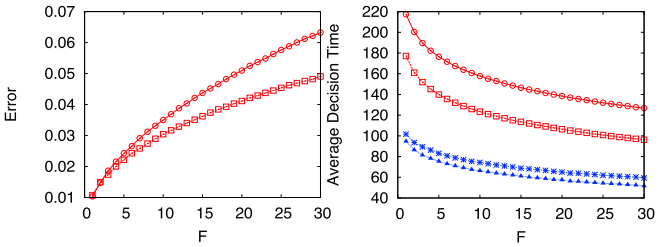

Fig. 5. The behavior of the biochemical Goldbeter–Koshland (GK) module for concentration discrimination (with a constant decay rate for E_2) compared with the optimal solution. The two ensembles that are compared have $\phi L_2 = 1.5$ vs. $\phi L_1 = 1$(the unbinding rate $\nu = 1$). For the leftmost points in the graphs ($F = 1$), the ratio of the kinetic parameters k_1 and k_2 appearing in Eq. **18** was fixed to have the critical values (where the GK module switches states and "decides") $(E_1/E_2)_{up} = 1{,}999$ and $(E_1/E_2)_{low} = 1.6\times10^{-3}$, which ensure 1% false positive and false negative errors. For the other points in the graphs, the upper/lower critical value was divided/multiplied by the factor F shown on the x axis. (*Left*) The classification error for data with $\phi L = 1.5$ (upper curve) and $\phi L = 1$ (lower curve) vs. F. (*Right*) The average decision times for the GK module (two upper curves) compared with the optimal solutions (two lower curves) vs. F. The thresholds for the Wald optimal solutions were adjusted to give the same error rate as the GK module with corresponding data. The slower/faster curves for each algorithm refer to data with $\phi L = 1.5/1$, respectively; e.g., red squares show GK presented with $\phi L = 1$.

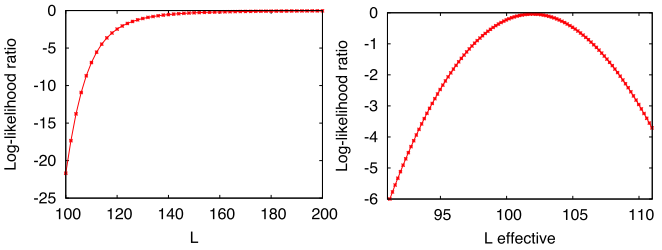

Fig. 6. The comparison between the full dynamics with receptors coupled and the dynamics with decoupled receptors and a fixed effective number L_{eff} of free ligands. For both panels the number of receptors is 100, $\phi = \nu = 1$. (*Left*) The log-likelihood ratio between the actual (coupled) model generating the data and the effective model vs. the total number of ligands L. (L_{eff} is optimized separately for each L.) The ratio is computed in the asymptotic regime at time 10. (*Right*) The behavior of the log-likelihood ratio vs. the effective number of free ligands L_{eff} around its maximum. The total number L of ligands is 200.

because it influences the distribution of z only when it is small. (In the derivation of Eqs. **14** and **15** we observed that a δ-function approximation for the weight around 0 was adequate in a continuum limit.) A more serious issue is molecular noise in the phosphorylation cascade leading to C_N. However, for N-Poisson events in series the SD in the sum scales as $\sqrt{N}$, so the time to activate C_N becomes sharper with N. To simulate Eq. **20**, one would sample the binding time t_i to the receptor and then compare it with the (random) time for transitioning from state $N-1$ to N, which is distributed according to the time derivative of Eq. **19**. The end result for Δz is manifestly a smoothed version of $\max(t_i - T, 0)$.

Biochemical Networks to Detect a Concentration Change Point. The optimal decision algorithm to detect a change in concentration, e.g., from L_1 to L_2, in a stream of data is governed by the same Eq. **11** derived previously but the probability ratio $R(t)$ in Eq. **5** is replaced by $L_2/L_1 e^{-\phi(L_2-L_1)t}$. This form simplifies the equation corresponding to Eq. **12**, which becomes

$$y_n = \log\left[\frac{L_2}{L_1(1-\lambda)}\right] - \phi(L_2 - L_1)t_n + \max(y_{n-1}, 0). \qquad [21]$$

Here, we have used again the approximation $\log(1+e^y) \simeq \max(y, 0)$ but the rest is now exact. Eq. **21** can be simulated biochemically by the same scheme as above, i.e., Eq. **20**.

Pooling the Output of Many Receptors. Having multiple receptors is clearly a bonus as it allows the cell to sample the ligand-binding statistics more rapidly and accelerates the decision process. Processing of information from receptor occupancy and calculating the optimal decision can be complicated, however, by coupling among receptors. This occurs when ligand sequestration effects are important, so that the likelihood of binding histories involves the configuration of the entire pool of receptors. Although these situations are possible, we show in Fig. 6 for the case of discriminating concentrations that a few-fold excess of ligands over the corresponding number of receptors is already sufficient to make an effective description with uncoupled receptors quite accurate.

Data are generated by Gillespie simulations of the binding/unbinding process for $R = 100$ receptors and a variable number of ligands L, Fig. 6. The number of nonoccupied receptors is denoted by $R_\varnothing$. We compare the log-likelihood ratio between the actual model generating the data [that depends on the instantaneous value of free ligands $L - R_o(t)$] and an effective model where free ligands are fixed at L_{eff}. Note that receptors are uncoupled for the latter model. Proceeding as for Eq. **3**, we obtain for the log-likelihood ratio of a trajectory extending up to time t,

$$\log\frac{P_{data}(t)}{P_{eff}(t)} = -\phi\left[\int_o^t (L - R + R_\varnothing(s))R_\varnothing(s)ds - \int_0^t L_{eff}R_\varnothing(s)ds\right] + \sum_{i=1}^{J_+}\log\frac{L - R + R_\varnothing(s_i)}{L_{eff}}, \qquad [22]$$

where s_i are the times when binding events occur and their total number up to time t is J_+. The graph of the log-likelihood ratio (for the best choice of L_{eff} at any given L) vs. the number of ligands L clearly shows that an effective description is accurate even for a twofold excess of ligands. Furthermore, the graph of the log-likelihoods vs. L_{eff} shows simple concave curves, the maximum of which is easy to find. Note that the best L_{eff} corresponding to the maximum is, as expected, close to the average number of free ligands $L - R + \overline{R}_\varnothing$, where $\overline{R}_\varnothing \leq R$ is the solution to the quadratic stationary equation $\phi(L - R + \overline{R}_\varnothing)\overline{R}_\varnothing = \nu(R - \overline{R}_\varnothing)$.

The biochemical models that we have developed above for a single receptor immediately generalize to many receptors if we decouple the receptors by using a fixed L_{eff}. For the discrimination of concentrations, it is for example sufficient that unbound/bound receptors additively contribute to the instantaneous decay rate of the two enzymes E_1/E_2. For the detection of a change in composition, the sequence of successive phosphorylations takes place on each individual receptor and then the endpoint, C_N, activities for all receptors are pooled to determine downstream events. Because receptors are independent for effective models, the rate of information acquisition is proportional to their number R and the average decision time will therefore reduce as $1/R$.

Discussion

The wealth of genetic and biochemical information about signaling pathways contrasts with the paucity of data on pathway dynamics. At the population level most data are interpreted around the paradigm that a ligand elicits a proportional response. The widespread realization that the same pathway is used in many different contexts, such as NFκB in inflammation and TGFβ in development, cancer, and immunology, does raise the question of whether pathways are more than passive transmission lines and in fact "compute" or act as dynamically reprogrammable filters (29). Posttranscriptional modifications of proteins are a natural substrate in which to implement analog chemical computation, and Jacob's old adage of bricolage suggests that signal transduction in cells might exploit this freedom to temporarily process signals. The canonical receptor systems as well as ion channels (30) possess a rich repertoire of interactions and modifications that could implement computation (31). One should note also a distinction between embryonic signaling where both the emitter and the receiver can be jointly tuned by evolution to process information and true environmental sensing where the signal has a more autonomous origin. Thus, in development, and even yeast mating, extracellular ligand processing may be as important as receptor interactions and posttranslational modifications in regulating pathway behavior (32, 33).

In the hope of stimulating experiments, and to explore the potential of analog biochemical computation in a concrete and nontrivial context, we have posed the problem of optimal decision theory for cells, in the context of detecting a change in concentration or composition. The problem is inherently dynamic, in that a stream of data is presented and a decision has to be made on the basis of the entire history. Thus, it is noteworthy, although simple to show, that optimal performance can be realized by accumulating a single variable in time. In a gene network context, it would seem

that decisions on the fly are much more natural than the alternative of averaging for a predefined time and then deciding, which has become the calculational default.

We have reduced the biochemical complexity of real systems to a ligand-binding step governed by equilibrium thermodynamics followed by downstream enzymology. More complexity is unnecessary because we have shown that ubiquitous small enzymatic systems suffice for near optimal performance. For the Wald problem, the ratio of two quantities, probabilities in our case, is naturally computed by the push–pull mechanism of Goldbeter and Koshland (27). The probabilities themselves are the exponential of a function of the input signal. Exponentials can be simulated with regulated decay and more speculatively by catalytic amplification. The most common amplification cascade as exemplified by phototransduction does not compute an exponential. What we require is the positive feedback of a transcriptional activator on itself with signal-dependent modulation, so that the factor grows exponentially in time. Using receptors that dimerize to signal, the same function could be realized if the dimers exchanged partners so that the fraction of active receptors grows exponentially (34).

The computation of change points can naturally be implemented with any system that encodes a time lag, such as a phosphorylation cascade. The computation is easiest for the log probability ratio, because the decision is one sided: When the indicator is large, decide; otherwise, continue. Thus, we do not have to take the ratio of two quantities and threshold separately on very small or very large values. A phosphorylation cascade is indeed observed in early T-cell activation yet the kinetic proofreading scheme is supplemented by the negative feedback by the phosphatase SH2 domain-containing tyrosine phosphatase (SHP-1) (35, 36). The functional reasons for this feedback are interesting.

T cells have to discriminate agonists from a far larger concentration of self antigens on the basis of only a three- to fivefold difference in off rates and plausibly do so quickly. This is analogous to our formulation of the mixture discrimination problem. However, in the immune system the total number of ligands can fluctuate, whereas we kept it fixed. Comparing the two schemes, the role of the negative feedback by SHP-1 appears then to buffer variations in the total concentration of ligands (36). The T cell also has to respond when a few agonists bind, whereas we have posed the mixture change-point problem with concentrations, so many receptors can be bound by agonist and yet not contribute to the decision. The optimal discrimination time T in Eq. **12** may be large enough to exclude most agonist binding events (recall in this context the heuristic argument for the nonanalytic decision time $\sim w^{-\alpha}$ after Eq. **8**).

We have focused on the decision process for a single receptor and it may be objected that cells are never challenged by the bounds we have placed on the decision time because they can always use many receptors in parallel and decide after a few on/off times. Even in this limit performance is improved by setting the receptor kinetic parameters as we have derived. Furthermore, we noted throughout the paper that decision times can easily become very long, e.g., 10^4 elementary events for a 1% discrimination in concentration. The cell may optimize subsets of receptors for various tasks by tuning cofactors or controlling access, and thus the number of receptors available in any one context may be less than the whole. Sheer increase of the number of receptors might therefore not be sufficient and evolving decision strategies as discussed here would be relevant to increase fitness.

How can one determine whether a cell is implementing a decision on the fly as opposed to computing for a fixed time? First, one would expect the decision time to scale with the strength of the signal. The high signal–short time limit would furnish a bound on the biochemical cascades induced by the receptor. Then for lower stimulation, does the decision time increase while the error rate remains fixed or does the opposite occur? Measuring a fractional power of w for the scaling of the decision time for the mixture change point when $\nu_1/\nu_2 > 2$ would be a good indication of optimality. Comparing the actual decision time with theory would be difficult due to uncertainties surrounding cellular parameters and variation among cells. The histogram of decision times is not Poisson and if well fitted by the data would suggest an optimal decision. More loosely, if one measured the distribution of several parameters that plausibly impact the signaling cascade and found their distribution individually is much broader than the distribution of decision times, it would be circumstantial evidence that the decision time is acting as a constraint on cell parameters.

Another class of tests uses microfluidics to flip the environment between the two states being compared. It would be possible to find conditions where a probability ratio test yielded a decision only after an immense time. The ability to control the environment dynamics and predict the consequences would be a strong check on the theory, but the details are very dependent on the experimental setup.

These considerations all apply to independent cells. Its an interesting and related question as to how a collection of interacting cells subject to a common external signal makes a rapid decision to respond, but as a collective with 100% participation. It is not obvious that the most rapid individual response followed by signaling to neighbors outperforms a more deliberate response at the cellular level with lower variance. Cell sorting is another response to signals that can contribute to the optimization problem. Thus, bounds on dynamics through statistical optimization may be a richer field of study in the cellular context than the physical limits to performance.

ACKNOWLEDGMENTS. E.D.S. was supported by National Science Foundation Grant PHY-0954398 and National Institutes of Health General Medical Sciences Award R01GM101653. M.V. was supported by the Fondation pour la Recherche Médicale (FRM) via Equipe FRM 2012 and by the Fondation de France T. Lebrasseur Award.

1. Wald A (1945) Sequential tests of statistical hypotheses. *Ann Math Stat* 16: 117–186.
2. Wald A (1947) *Sequential Analysis* (Wiley, New York).
3. DeGroot MH (2004) *Optimal Statistical Decisions* (Wiley, New York).
4. Parmigiani G, Inoue L (2009) *Decision Theory. Principles and Approaches* (Wiley, New York).
5. Shiryaev AN (1963) On the detection of disorder in a manufacturing process. I. *Theory Probab Appl* 8(3):247–265.
6. Shiryaev AN (1963) On the detection of disorder in a manufacturing process. II. *Theory Probab Appl* 8(4):402–413.
7. Shiryaev AN (1963) On optimum methods in quickest detection problems. *Theory Probab Appl* 8:22–46.
8. Vergassola M, Villermaux E, Shraiman BI (2007) 'Infotaxis' as a strategy for searching without gradients. *Nature* 445(7126):406–409.
9. Uchida N, Kepecs A, Mainen ZF (2006) Seeing at a glance, smelling in a whiff: Rapid forms of perceptual decision making. *Nat Rev Neurosci* 7(6):485–491.
10. Gold JI, Shadlen MN (2007) The neural basis of decision making. *Annu Rev Neurosci* 30:535–574.
11. Bogacz R, Brown E, Moehlis J, Holmes P, Cohen JD (2006) The physics of optimal decision making: A formal analysis of models of performance in two-alternative forced-choice tasks. *Psychol Rev* 113(4):700–765.
12. Kobayashi TJ (2010) Implementation of dynamic Bayesian decision making by intracellular kinetics. *Phys Rev Lett* 104(22):228104.
13. Kobayashi TJ, Kamimura A (2011) Dynamics of intracellular information decoding. *Phys Biol* 8(5):055007.
14. Ziv E, Nemenman I, Wiggins CH (2007) Optimal signal processing in small stochastic biochemical networks. *PLoS ONE* 2(10):e1077.
15. Tkacik G, Callan CG, Jr., Bialek W (2008) Information flow and optimization in transcriptional regulation. *Proc Natl Acad Sci USA* 105(34):12265–12270.
16. Tostevin F, ten Wolde PR (2009) Mutual information between input and output trajectories of biochemical networks. *Phys Rev Lett* 102(21):218101.
17. Bousso P, Robey EA (2004) Dynamic behavior of T cells and thymocytes in lymphoid organs as revealed by two-photon microscopy. *Immunity* 21(3):349–355.
18. Krishna S, Maslov S, Sneppen K (2007) UV-induced mutagenesis in Escherichia coli SOS response: A quantitative model. *PLoS Comput Biol* 3(3):e41.
19. Berg HC (2003) *E. coli in Motion* (Springer, New York).

20. Takeda K, et al. (2012) Incoherent feedforward control governs adaptation of activated ras in a eukaryotic chemotaxis pathway. *Sci Signal* 5(205):ra2.
21. Brivanlou AH, Darnell JE, Jr. (2002) Signal transduction and the control of gene expression. *Science* 295(5556):813–818.
22. Lemmon MA, Schlessinger J (2010) Cell signaling by receptor tyrosine kinases. *Cell* 141(7):1117–1134.
23. Cover TN, Thomas JA (2006) *Elements of Information Theory* (Wiley, New York).
24. Berg HC, Purcell EM (1977) Physics of chemoreception. *Biophys J* 20(2):193–219.
25. Endres RG, Wingreen NS (2009) Maximum likelihood and the single receptor. *Phys Rev Lett* 103(15):158101.
26. Aldous D (1989) *Probability Approximations via the Poisson Clumping Heuristic* (Springer, New York).
27. Goldbeter A, Koshland DE, Jr. (1981) An amplified sensitivity arising from covalent modification in biological systems. *Proc Natl Acad Sci USA* 78(11): 6840–6844.
28. Cookson NA, et al. (2011) Queueing up for enzymatic processing: Correlated signaling through coupled degradation. *Mol Syst Biol* 7:561.
29. Behar M, Hoffmann A (2010) Understanding the temporal codes of intra-cellular signals. *Curr Opin Genet Dev* 20(6):684–693.
30. Hwang TC, Kirk KL (2013) The CFTR ion channel: Gating, regulation, and anion permeation. *Cold Spring Harb Perspect Med* 3(1):a009498.
31. Hao N, O'Shea EK (2012) Signal-dependent dynamics of transcription factor translocation controls gene expression. *Nat Struct Mol Biol* 19(1):31–39.
32. Beachy PA, Hymowitz SG, Lazarus RA, Leahy DJ, Siebold C (2010) Interactions between Hedgehog proteins and their binding partners come into view. *Genes Dev* 24(18):2001–2012.
33. Jin M, et al. (2011) Yeast dynamically modify their environment to achieve better mating efficiency. *Sci Signal* 4(186):ra54.
34. Chao LH, et al. (2010) Intersubunit capture of regulatory segments is a component of cooperative CaMKII activation. *Nat Struct Mol Biol* 17(3):264–272.
35. Altan-Bonnet G, Germain RN (2005) Modeling T cell antigen discrimination based on feedback control of digital ERK responses. *PLoS Biol* 3(11):e356.
36. François P, Voisinne G, Siggia ED, Altan-Bonnet G, Vergassola M (2013) Phenotypic model for early T-cell activation displaying sensitivity, specificity, and antagonism. *Proc Natl Acad Sci USA* 110(10):E888–E897.

Supplementary Information "Decisions on the fly in biological sensory systems"

Eric D. Siggia & Massimo Vergassola

July 21, 2013

1 Occupation statistics for a receptor

The aim of this Section is the derivation of the occupancy statistics for the Poisson process of binding/unbinding of a ligand to its receptor. Results will allow us to obtain analytical expressions for the Wald decision time in the approximation when the log-likelihood is well approximated by a diffusive process with drift (see below).

We denote the total number of jumps by $J = J_+ + J_-$ where J_+ and J_- indicate number of jumps upward (binding) and downward (unbinding), respectively. The Boolean receptor occupancy variable $n(t)$ is related to the jumps as $n(t) = n(0)+J_+(t)-J_-(t)$. We shall use n and J as our independent variables, with J_+ and J_- obtained via the previous expressions.

The master equations for the probability $P(n, J, t)$ are

$$\begin{aligned} \frac{\partial P(1,J,t)}{\partial t} &= \phi L\, P(0,J-1,t) - \nu\, P(1,J,t)\,; \\ \frac{\partial P(0,J,t)}{\partial t} &= \nu\, P(1,J-1,t) - \phi L\, P(0,J,t)\,. \end{aligned} \tag{1}$$

Since $\langle n\rangle(t) = \sum_J P(1,J,t)$, we obtain the two equations

$$\begin{aligned} \frac{d\langle n\rangle}{dt} &= \phi L\, (1-\langle n\rangle) - \nu\, \langle n\rangle\,; \\ \frac{d\langle J\rangle}{dt} &= \phi L\, (1-\langle n\rangle) + \nu\, \langle n\rangle\,. \end{aligned} \tag{2}$$

After the initial transient relaxation (taking place at the rate $\nu + \phi L$), the averages converge to their steady-state expressions

$$\langle n \rangle \simeq \frac{\phi L}{\phi L + \nu}\,; \quad \frac{d\langle J \rangle}{dt} \simeq \frac{2\nu\phi L}{\phi L + \nu}\,; \quad \frac{d\langle J_+ \rangle}{dt} \simeq \frac{d\langle J_- \rangle}{dt} \simeq \frac{1}{2}\frac{d\langle J \rangle}{dt}\,. \tag{3}$$

As for second-order correlations, algebraic manipulations of the Eqs. 1 yield

$$\begin{aligned}
\frac{dC_{nn}(t,s)}{dt} &= -\left(\nu + \phi L\right) C_{nn}(t,s)\,; \; \frac{dC_{nJ}(t,s)}{dt} = -\left(\nu + \phi L\right) C_{nJ}(t,s)\,; \\
\frac{dC_{Jn}(t,s)}{dt} &= \left(\nu - \phi L\right) C_{nn}(t,s)\,; \; \frac{dC_{JJ}(t,s)}{dt} = \left(\nu - \phi L\right) C_{nJ}(t,s)\,,
\end{aligned} \tag{4}$$

for the connected correlations, e.g. $C_{nJ}(t,s) \equiv \langle n(t)\, J(s) \rangle - \langle n(t) \rangle \langle J(s) \rangle$, etc., where $t \neq s$. Equal-time correlations are obtained similarly :

$$\begin{aligned}
C_{nn}(t,t) &= \langle n(t) \rangle \left(1 - \langle n(t) \rangle\right)\,; \\
\frac{dC_{nJ}(t,t)}{dt} &= \phi L \left(1 - \langle n(t) \rangle\right)^2 - \left(\nu + \phi L\right) C_{nJ}(t,t) - \nu \langle n(t) \rangle^2\,; \\
\frac{dC_{JJ}(t,t)}{dt} &= 2\left(\nu - \phi L\right) C_{nJ}(t,t) + \nu \langle n(t) \rangle + \phi L \left(1 - \langle n(t) \rangle\right)\,.
\end{aligned} \tag{5}$$

The solution of the Eqs. 4 is lengthy but straightforward. The expressions needed to compute drift and diffusivity of the log-likelihood are the following :

$$C_{nn}(t-s) = \frac{\phi L \nu}{\left(\phi L + \nu\right)^2} e^{-(\phi L + \nu)|t-s|}\,; \tag{6}$$

$$C_{nJ}(t-s) = \frac{\phi L \nu}{\left(\phi L + \nu\right)^3} \left(\nu - \phi L\right) e^{-(\phi L + \nu)(t-s)} \quad t \geq s\,; \tag{7}$$

$$C_{Jn}(t-s) = \frac{\phi L \nu}{\left(\phi L + \nu\right)^3} \left(\nu - \phi L\right) \left[2 - e^{-(\phi L + \nu)(t-s)}\right] \quad t \geq s\,; \tag{8}$$

$$C_{JJ}(t,t) \simeq 4\frac{\phi L \nu}{\left(\phi L + \nu\right)^3} \left(\nu^2 + \phi^2 L^2\right) t \quad \text{for } t \text{ large}\,. \tag{9}$$

The expressions are valid after the relaxation of the initial transients.

For the discrimination of concentration levels, the log-likelihood ratio for the two hypotheses reads :

$$\ln\left(\frac{P(L_2)}{P(L_1)}\right) = -\phi(L_2 - L_1) \int_0^t \left(1 - n\left(s\right)\right)\, ds + J_+(t) \ln\left(\frac{L_2}{L_1}\right)\,. \tag{10}$$

The current time is denoted by t, the number of jumps upward by $J_+(t)$ and the occupancy Boolean variable (1 and 0 corresponding to the receptor being occupied/unoccupied, respectively) by $n(t)$. Drift and diffusivity are obtained via the receptor occupancy statistics presented above. The expression for the drift reads:

$$\frac{d}{dt}\langle \ln\left(\frac{P(L_2)}{P(L_1)}\right)\rangle = \frac{\nu\phi}{\nu+\phi L}\left[L_1 - L_2 + L\ln\left(\frac{L_2}{L_1}\right)\right], \tag{11}$$

where we have used Eq. 3. The concentration L corresponds to the real process generating the data (the value of which can possibly differ from L_1 and/or L_2 in the case when the two tested models are not exact). The square of Eq. 10 gives for the diffusivity

$$\begin{aligned} D = \frac{1}{2}\left[\frac{d}{dt}\langle \ln\left(\frac{P(L_2)}{P(L_1)}\right)^2\rangle - \frac{d}{dt}\langle \ln\left(\frac{P(L_2)}{P(L_1)}\right)\rangle^2\right] = \\ \frac{\nu\phi L}{(\nu+\phi L)^3}\left[(\phi\,(L_2-L_1))^2 + \frac{1}{2}\ln^2\left(\frac{L_2}{L_1}\right)\left(\nu^2+\phi^2L^2\right)\right. \\ \left. +\phi(L_2-L_1)\ln\left(\frac{L_2}{L_1}\right)(\nu-\phi L)\right]. \end{aligned} \tag{12}$$

The comparison between Eqs. 11 and 12 and average and variance of the log-likelihood obtained by Monte-Carlo numerical data is shown in Fig. S1. The excellent comparison between the Wald average decision time and its diffusion approximation, given by the upcoming Eq. 15, is shown in the main text.

2 Absorption time for a diffusive process

We consider here a stochastic process diffusing and drifting with a constant velocity. Two absorbing boundaries are present on the two sides of the starting position so that the particle is eventually absorbed. By using standard first-passage methods (see, e.g., [1]), we derive here the expression for the average time of absorption. The two absorbing boundaries are taken at $\pm K$ (this entails no limitation as symmetric boundaries can always be achieved by an appropriate choice of the origin). The starting position in the corresponding system of coordinates is denoted x. The average time of absorption

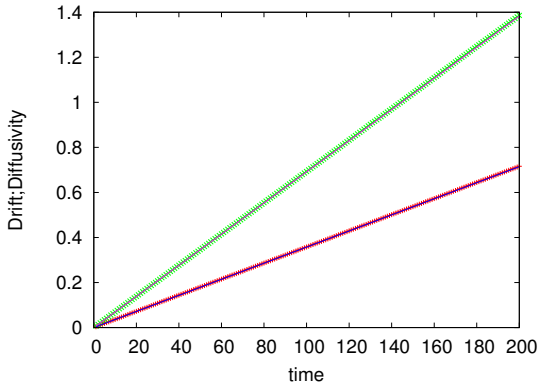

Figure 1: The behavior of log-likelihood average (lower red curve) and variance (upper green curve) as a function of time for $\phi L = \phi L_2 = 2$, $\phi L_1 = 1.8$ and $\nu = 1$. The fitting straight lines correspond to the values of drift and diffusivity in Eqs. 11 and 12.

$\langle T_{\rm abs}\rangle(x)$ satisfies the backward Kolmogorov equation

$$\left(D\frac{d^2}{dx^2} + V\frac{d}{dx}\right)\langle T_{\rm abs}\rangle(x) = -1\,. \tag{13}$$

The general solution of Eq. 13 reads

$$\langle T_{\rm abs}\rangle(x) = -\frac{x}{V} + C_1 + C_2 e^{-x\frac{V}{D}}\,. \tag{14}$$

The two arbitrary constants C_1 and C_2 are fixed by the boundary conditions $\langle T_{\rm abs}\rangle(x = \pm K) = 0$ and we obtain the final expression

$$\langle T_{\rm abs}\rangle(K,x) = -\frac{x}{V} + \frac{K}{2V\sinh\left(VK/D\right)}\left[e^{\frac{KV}{D}} + e^{-\frac{KV}{D}} - 2e^{-x\frac{V}{D}}\right]\,. \tag{15}$$

One can also easily compute the Laplace transform $Q(s,x)$ of the absorption time, which obeys

$$\left(D\frac{d^2}{dx^2} + V\frac{d}{dx}\right)Q(s,x) = sQ(s,x)\,. \tag{16}$$

Solving Eq. 16 and noting that for $x = \pm K$ the absorption time distribution is a Dirac-δ at the origin, we obtain

$$Q(s,x) = \frac{e^{-\frac{V}{2D}(x+K)}\sinh\left(\Delta\left(K-x\right)\right) + e^{-\frac{V}{2D}(x-K)}\sinh\left(\Delta\left(K+x\right)\right)}{\sinh\left(2K\Delta\right)}\,, \tag{17}$$

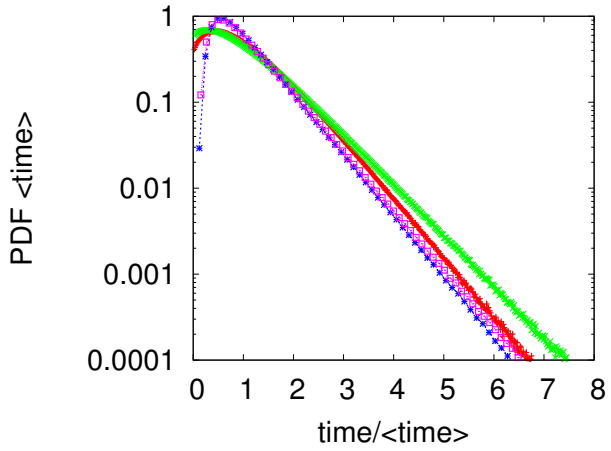

Figure 2: The PDFs (multiplied by their respective means) of the decision time (rescaled by its mean) for the Ratio Test for concentrations (blue and purple curves) and the Change Point for mixtures (green and red curves). Parameters for the former, as defined in the body of the paper, are: $\nu = 1$, $\phi L_2 = 1$, $\phi L_1 = 1.1$ (blue) and $\phi L_1 = 1.5$ (purple), data are sampled with an on-rate $\phi L = 1$ and precisions (false positive and false negative fractions) are 1%. Parameters for the mixture problem, as defined in the body of the paper, see Eqs. 11 and 16, are as follows. The mixture is generated with three frequencies $\nu_1 = 1$, $\nu_2 = 1.5$ and $\nu_3 = 2$ and its composition is uniform. The agonist species with $\nu_a = 0.3$, $w = 0.1$ is added to the mixture at a Poisson distributed time with mean $1/\lambda = 100$ in iteration units. The red curve is for a precision (false positive detections, prior to the adding of the agonist species) of 1% whilst the green one is for 5%.

where $\Delta \equiv \frac{\sqrt{V^2+4Ds}}{2D}$. Moments of the absorption time can be obtained by taking derivatives of Eq. 17 with respect to s at $s = 0$.

The Probability Distribution Function (PDF) of decision times for the Ratio Test for Concentrations and the Change Point for Mixtures are shown in Fig. S2 and feature the expected exponential behavior for values larger than the mean.

3 Probabilities of absorption

We consider the same problem as in the previous Section but derive here the expression for the probability of being absorbed on one specific boundary. The probability of absorption at the boundary in K satisfies

$$\left(D\frac{d^2}{dx^2} + V\frac{d}{dx} \right) \mathcal{P}(x, K) = 0\,. \tag{18}$$

Here, x is the initial value of the process and the boundary conditions are $\mathcal{P}(K, K) = 1$ and $\mathcal{P}(-K, K) = 0$. The solution of the Eq. 18 reads

$$\mathcal{P}(x, K) = \frac{e^{\frac{VK}{D}} - e^{-\frac{Vx}{D}}}{e^{\frac{VK}{D}} - e^{-\frac{VK}{D}}}\,. \tag{19}$$

The probability $\mathcal{P}(x, -K) = 1 - \mathcal{P}(x, K)$.

4 Absorption time for Wald decisions

The Sequential Probability Ratio Test (SPRT) introduced by A. Wald [2], is meant to discriminate between two different statistical hypotheses. The method involves the calculation of the log-likelihood ratio between the two alternatives and prescribes continuation of data acquisition as long as the likelihood ratio $K_- < P_2/P_1 < K_+$, where $K_- < K_+$ are two fixed boundary levels. Decision is made when one of the two boundaries is passed, the first (second) hypothesis being called if $P_2/P_1 \leq K_-$ ($P_2/P_1 \geq K_+$).

Let us define by $e_{i|j}$ the probability that generating data with the model j the (wrong) decision is made for the alternative model i. We fix the two boundaries K_- and K_+ in such a way that the errors for SPRT are $e^*_{1|2}$ and $e^*_{2|1}$ (see Section 5). SPRT is optimal in the following sense: any other decision procedure that ensures $e_{1|2} \leq e^*_{1|2}$ and $e_{2|1} \leq e^*_{2|1}$ will have a longer average time for decision.

For long enough times, the dynamics of the decision process simplifies as we expect that the log-likelihood ratio between two hypotheses will be well approximated by its approximation as a Gaussian diffusion with drift. The starting value of the log-likelihood is at zero (for a flat prior) and the two boundaries are located at $\log K_-$ (negative) and $\log K_+$ (positive) – the relation of the boundaries to the errors is discussed below. It is easily

checked that this problem is mapped into symmetric absorbing boundaries (as in the two previous Sections) by taking the initial starting position at $x = -\frac{\log K_+ + \log K_-}{2}$ and setting the threshold $K = \frac{\log K_+ - \log K_-}{2}$. The average decision time and the Laplace transform for the absorption time are then read directly with the previous substitutions.

5 Absorbing boundaries in Wald decisions

The goal of this Section is to discuss how the boundaries K_- (negative) and K_+ (positive) for the likelihood ratio P_2/P_1, are related to the false positive and false negative errors.

Let us start by considering the case where the desired errors are low enough that the log-likelihoods at the typical absorption times are well described by the corresponding diffusive approximations. We can then use the formulas derived in Section 3 to choose appropriately K so as to have the desired errors. We remind that the formulas in Section 3 are related to the Wald decision problem by having the initial starting position at $x = -\frac{\log K_+ + \log K_-}{2}$ and the threshold $K = \frac{\log K_+ - \log K_-}{2}$.

If the diffusive approximation does not apply, it is still possible to derive explicit expressions in the case where the log-likelihood process is continuous and does not feature strong jumps (on the scale of the boundaries). Proceeding as in the original paper by Wald, we consider a trajectory that reaches the lower boundary K_- (without having touched beforehand the two boundaries). Continuity implies that at the passage time $P_2/P_1 \simeq K_-$. We now integrate over all possible trajectories $\{x\}$ of the log-likelihood, weighting them with the probability of the first statistical hypothesis, i.e. P_1. It follows that $\int_- P_2(\{x\})\mathcal{D}\{x\} = K_- \int_- P_1(\{x\})\mathcal{D}\{x\}$, where $\int_-$ indicates that the integrals are restricted to those trajectories $\{x\}$ that hit first the lower boundary. We conclude that $e_{1|2} = K_- \left(1 - e_{2|1}\right)$ where $e_{i|j}$ is the probability that generating trajectories with the model j the (wrong) decision is made for the alternative model i. Considering the reciprocal case of the first passage at the upper boundary $P_1/P_2 \simeq 1/K_+$ and integrating over the trajectories with the P_2 weights, we obtain K_+. The final expressions of the two boundaries read

$$K_+ = \frac{1 - e_{1|2}}{e_{2|1}}\,, \qquad K_- = \frac{e_{1|2}}{1 - e_{2|1}}\,. \tag{20}$$

Finally, if the process features strong jumps and continuity is not ensured, then the choice of the two decision boundaries must generally proceed on an empirical basis, varying the two thresholds and looking for the desired error levels.

6 Fixed sample size Maximum Likelihood decisions

The goal of this Section is to briefly recall how Maximum Likelihood decisions are made in the standard case when a fixed sample size is considered. The length of the sample is determined so as to ensure the desired level of accuracy and, contrary to the Wald case discussed in previous Sections, is fixed. We shall briefly present the case of discriminating concentration levels as an example and refer to [2] for more details. The specific purpose is to provide details as to how the Maximum Likelihood curve in Fig. 1 of the paper is obtained.

As shown in previous Sections, the variable $v = \frac{1}{t}\log P(L_2)/P(L_1)$ is approximately Gaussian at long enough times. When data are generated with concentrations $L = L_1$ or $L = L_2$, the corresponding mean value $V_{1,2}$ and variances $2D_{1,2}/t$ at time t are given by the expressions (11) and (12) with $L = L_1$ or $L = L_2$, respectively. It follows from Neyman-Pearson lemma (see, e.g., [3]) that we should impose a threshold v^* on the log-likelihood ratio and call L_2 if $v > v^*$ and L_1 vice versa. The corresponding errors for long enough t (and for fluctuations that do not involve large deviations from the mean) read

$$e_{2|1}^{ML} = \int_{\sqrt{\frac{t}{4D_1}}(v^*-V_1)}^{\infty} \frac{e^{-z^2}}{\sqrt{\pi}}\,; \quad e_{1|2}^{ML} = \int_{\sqrt{\frac{t}{4D_2}}(V_2-v^*)}^{\infty} \frac{e^{-z^2}}{\sqrt{\pi}}\,. \tag{21}$$

If the two desired errors are equal $e_{2|1}^{ML} = e_{1|2}^{ML} = \varepsilon$, then $v^* = \frac{V_1\sqrt{D_2}+V_2\sqrt{D_1}}{\sqrt{D_1}+\sqrt{D_2}}$ and it follows from (21) that the fixed sample size t_{ML}^* is defined by the equation

$$\mathrm{erfc}\left(\sqrt{\frac{t_{ML}^*}{4}}\frac{V_2-V_1}{\sqrt{D_1}+\sqrt{D_2}}\right) = 2\varepsilon\,, \tag{22}$$

where erfc is the complementary error function. For the precision $\varepsilon = 0.01$,

we have $t^*_{ML} \simeq 4 \times 1.645^2 \left(\frac{\sqrt{D_1}+\sqrt{D_2}}{V_2-V_1}\right)^2$, which is the curve appearing in Fig. 1 of the paper.

7 A (oversimplified) model for discrimination of mixtures

A possible formulation of the mixture problem runs parallel to the case of discriminating concentrations but we show here that it needs improvement. Let us assume that the smallest dissociation time of foreign ligands that we want to detect is ν_2^{-1} and that the longest dissociation time of self ligands is ν_1^{-1}. We can then try discriminating the two simple hypotheses: (I) pure ligands, i.e. L ligands with unbinding rate ν_1 *vs* (II) $L - \delta L$ ligands with unbinding rate ν_1 and δL with unbinding rate ν_2. The corresponding ratio of the two likelihoods reads

$$\ln\left(\frac{P_2}{P_1}\right) = \sum_b \log\left[(1-w) + we^{-(\nu_2-\nu_1)t_b}\,\mathcal{U}\left(\frac{\nu_2}{\nu_1}\right)\right], \tag{23}$$

where t_b are the intervals of time that the receptor was (or is being) occupied, the sum runs over them, $w \equiv \delta L/L$ and the factor $\mathcal{U} = \nu_2/\nu_1$ for all of the terms in the sum but (possibly) the last one. If the binding is still ongoing at the current time t, no factor should indeed be included and $\mathcal{U} = 1$. The unoccupied periods do not contribute to the discrimination as the concentrations and the binding rates are the same for the two hypotheses to discriminate.

In the body of the paper we derived the asymptotic behavior for average of Eq. 23 in the limit of small w. Here, we note that the integrals for the average have an exact closed form in terms of hypergeometric functions. Using Formula 3.194.2 of [4] it is for example possible to compute the average for a pure state

$$\langle R\rangle_p = \nu_1 \int e^{-\nu_1 t_b} \log\left((1-w) + we^{(\nu_1-\nu_2)t_b}\frac{\nu_2}{\nu_1}\right) dt_b\,, \tag{24}$$

as

$$\begin{aligned}\langle R\rangle_p &= \log\left(1 - w + w\frac{\nu_2}{\nu_1}\right) \\ &+ \left(1-\frac{\nu_2}{\nu_1}\right) {}_2F_1\left(1, \frac{\nu_1}{\nu_1-\nu_2}, \frac{2\nu_1-\nu_2}{\nu_1-\nu_2}\,; -\frac{\nu_1\,(1-w)}{w\nu_2}\right).\end{aligned} \tag{25}$$

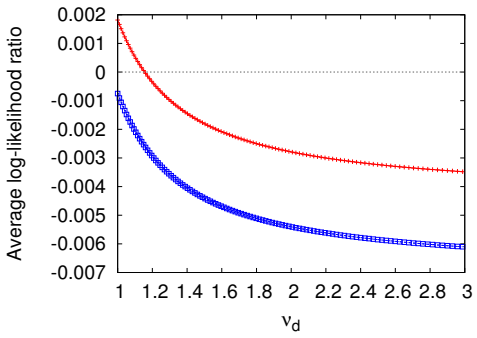

Figure 3: The average of the log likelihood ratio between pure and mixture models. The models have $\delta L/L = 0.01$, $\nu_1 = 1$ and $\nu_2 = 0.3$. Data are generated with the self unbinding rate ν indicated on the abscissae; the red curve refers to data generated with 99% self (rate ν) and 1% foreign (rate ν_2) whilst the green one refers to data generated with 100% self (rate ν). Note that the red curve starts with a positive value, i.e. the mixture model is favored, as it should, yet it becomes negative as ν increases.

Similar formulas can be obtained for the average of the mixture.

The pitfall of the simple model Eq. 23 is illustrated in Fig. S3. If data are generated with a mixture but self has unbinding rate $\nu \geq \nu_1$, the comparison between the pure and mixture models with the self unbinding rate set at ν_1 will favor the pure model.

This effect, which seems counter intuitive at first, is in fact readily explained in Fig. S4 where we plot the integral

$$I(T) = \int_0^T \left[w\,\nu_2\,e^{-\nu_2 t} + (1-w)\,\nu e^{-\nu t}\right] \times \log\left[(1-w) + \frac{\nu_2\,w}{\nu_1} e^{(\nu_1-\nu_2)t}\right] dt\,. \tag{26}$$

Note that for $T \to \infty$ the integral gives the expected value of the log likelihood ratio plotted in Fig. S3, i.e. we are plotting how different binding times contribute to the average. It is clear then that long-binding events are favoring the mixture as expected, yet the contribution is counterbalanced by the contribution coming from short-binding events, which are even more frequent than expected under the pure model. Since short-binding events

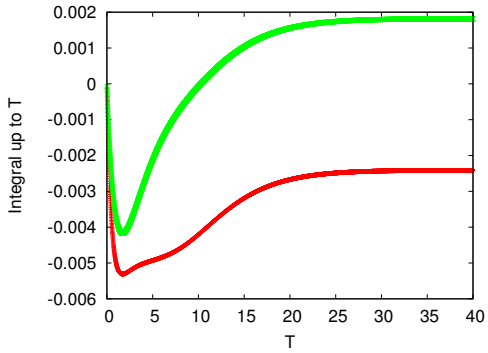

Figure 4: The integral defined in Eq. 26, indicating how different binding times contribute to the average of the log likelihood ratio between pure and mixture models having $\delta L/L = 0.01$, $\nu_1 = 1$ and $\nu_2 = 0.3$. Data for the green curve are generated with the same parameters whilst those for the red one are generated with $\nu = 1.75$.

are more numerous than long ones, they end up contributing more than the latter and the final sign is negative.

8 Long-time approximation for discriminating mixtures

As discussed in the body of the paper, an appropriate formulation of the discrimination problem is between the following two hypotheses: (I) pure self, i.e. *any* distribution of ligands having rates $\geq \nu_s$ (total concentration L); (II) a fraction $w_f = \delta L/L$ having unbinding rate $\leq \nu_f$ and the rest of the mixture composed of *any distribution* of ligands having rates $\geq \nu_s$ (total concentration $L - \delta L$). The log-likelihood ratio of the two hypotheses reads

$$\ln\left(\frac{P_2}{P_1}\right) = \log\left[\frac{\int d\boldsymbol{w}\prod_b \mathcal{L}(t_b\,|w_f,\boldsymbol{w})\delta(w_f+\sum_j w_j-1)}{\int d\boldsymbol{w}\prod_b \mathcal{L}(t_b\,|\boldsymbol{w})\delta(\sum_j w_j-1)}\right], \tag{27}$$

where the likelihoods for a given binding time t_b are

$$\mathcal{L}(t_b\,|w_f,\boldsymbol{w}) = w_f e^{-\nu_f t_b}\nu_f + \sum_{j=1}^{M} w_j e^{-\nu_j t_b}\nu_j\,,$$
$$\mathcal{L}(t_b\,|\boldsymbol{w}) = \sum_{j=1}^{M} w_j e^{-\nu_j t_b}\nu_j\,. \tag{28}$$

The sums run over the M self types having dissociation rates $\nu_1,\ldots,\nu_M$. All self dissociation rates obey $\nu_j \geq \nu_s$ and the limit of a continuum might of course be taken as $M\to\infty$. Eqs. 28 are valid for all binding events but possibly the last one. Indeed, if the binding is still ongoing at the current time t, then $t_b = t - t_{on}$, where t_{on} is the time of the last binding event, and there are no factors ν_f and ν_j in Eq. 28 since the eventual unbinding has not occurred yet. We have assumed that no prior information is available, i.e. a flat distribution on the weights $\boldsymbol{w}$.

For times much longer than the typical times of binding and unbinding, the number of binding events B is very large and the sequence of binding times in a given realization will be distributed according to large deviation theory. The so-called empirical distribution $P(t_b)$ is the relative occurrence of a certain binding time t_b in the sequence. From the method of types, see, e.g. [3], it follows that empirical distributions for a long sequence of binding times will be peaked around the most probable distribution $Q(t_b)$ that generates data. The probability for deviations of the empirical $P(t_b)$ from $Q(t_b)$ decays exponentially in B as $\exp[-BH(Q||P)]$, where $H(Q||P) = \int dt_b Q(t_b)\log\left(Q/P\right)(t_b)$ is the Kullback-Leibler entropy. Moreover, the Bayesian integrals in Eq. 27 are expected to be dominated by their saddle contributions and their logarithms should thus be proportional to B (logarithmic corrections will be discussed momentarily). It follows that moments of log-likelihood ratios will be dominated by $Q(\tau_b)$ and we conclude that

$$\langle\log\int d\boldsymbol{w}\; e^{\sum_b \ln\mathcal{L}(t_b|\boldsymbol{w})}\delta(\sum_j w_j - 1)\rangle \simeq B\langle\ln\mathcal{L}\rangle(\boldsymbol{w}^*) - \beta\ln B + \ldots\,, \tag{29}$$

where $\boldsymbol{w}^*$ are the weights that maximize the term at the exponential $\langle\ln\mathcal{L}(\boldsymbol{w})\rangle$ and averages are computed with respect to the distribution $Q(t_b)$ generating the data. Other averages of log-likelihoods are estimated similarly.

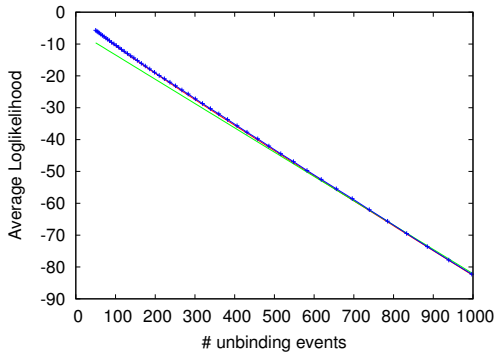

Figure 5: The behavior of the average log-likelihood defined in Eq. 31 with binding times generated by the distribution $Q(t_b) = w_f e^{-\nu_f t_b}\nu_f + (1 - w_f)e^{-\nu_3 t_b}$. The model has three components $M = 3$, with $w_f = 0.1$, $\nu_f = 0.3$, $\nu_1 = \nu_s = 1$, $\nu_2 = 2$, $\nu_3 = 3$. The two-dimensional Bayesian integrals are computed by Simpson method. The green line is the power-law in Eq. 29 (and an adjusted constant). The blue line (which coincides with Monte-Carlo data) includes a logarithmic correction with $\beta = 1.5$ since a single component of the gradient at the extremum is non-zero.

Logarithmic corrections in Eq. 29 will depend on the nature of the extremum $\boldsymbol{w}^*$. For data generated by a probability distribution which features only unbinding rates included in the model, it is easy to show that $\boldsymbol{w}^*$ correspond to the generating weights. Specifically, if $Q(t_b) = \sum_{j=1}^{M} W_j e^{-\nu_j t_b}\nu_j$ (with $\sum_j W_j = 1$), then the extremum of

$$\int Q(t_b) \log \left[\frac{\sum_j w_j e^{-\nu_j t_b}\nu_j}{Q(t_b)} \right] dt_b + \lambda \left(\sum_j w_j - 1 \right) , \tag{30}$$

is $w_j^* = W_j$. If the expression at the exponential behaves quadratically around its maximum, the constant in Eq. 29 asymptotically approaches $\beta = (M-1)/2$.

When data and models do not correspond, i.e. there is no choice of the model weights $\boldsymbol{w}$ such that $Q(t_b) = \sum_j w_j e^{-\nu_j t_b}\nu_j$, the saddle point is not obvious and numerics is needed. The maximum might be a true extremum or be at the boundary of the interval of definition ($0 \leq w_j \leq 1$ and $\sum_j w_j$ fixed) with a non-vanishing gradient. The constant β will then depend on the number of non-zero components in the gradient. For example, $\beta = M-1$

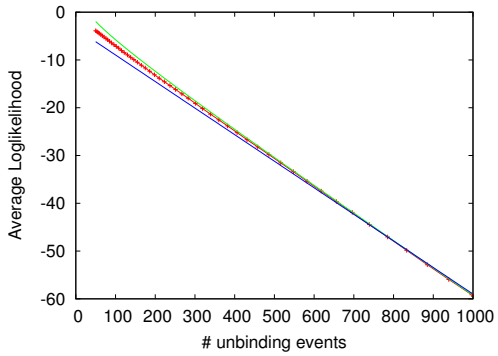

Figure 6: The behavior of the average log-likelihood defined in Eq. 31 with binding times generated by the distribution $Q(t_b) = w_f e^{-\nu_f t_b}\nu_f + (1 - w_f)\nu_2 e^{-\nu_2 t_b}$. The model has three components $M = 3$, with $w_f = 0.1$, $\nu_f = 0.3$, $\nu_1 = 1$, $\nu_2 = 2$, $\nu_3 = 3$. The two-dimensional Bayesian integrals are computed by Simpson method. The blue line is the power-law in Eq. 29 (and an adjusted constant). The green line includes a logarithmic correction with $\beta = 1.5$ since a single component of the gradient at the extremum is non-zero. The red line are MonteCarlo simulation data.

for an extremum on the boundary with all independent components of the gradient non-vanishing. An example of such situation is $Q(t_b) = w_f e^{-\nu_f t_b}\nu_f + (1 - w_f)e^{-\nu_s t_b}\nu_s$ and a model of self with the first component ν_s and all the other $\nu_j > \nu_s$. Intermediate cases interpolate between the previous two extreme cases, see e.g. Fig. S5 where we plot

$$I = \int Q(t_b) \log \left[\frac{\int d\boldsymbol{w}\; e^{\sum_b \ln \mathcal{L}(t_b|\boldsymbol{w})} \delta(\sum_j w_j - 1)}{Q(t_b)} \right] dt_b \,. \tag{31}$$

There are other cases where the behavior at moderate times is even more affected by finite-size effects, see Fig. S6. The conclusion from the figures is that for discriminations down to precision $O(1\%)$ (which corresponds to differences in log likelihoods of several units yet not several tens) drift and diffusivity will change substantially during the decision process time span and the applicability of the diffusion approximation is more limited than in the case of detecting concentration differences.

9 Detecting the time of mixing

In this Section we solve for a piecewise linear approximation to the recursion formula for sensing the time when a longer lived species is mixed into the background while preserving the total concentration. For a single receptor we can time slice the path integral when the ligand falls off. If the occupancy time of a ligand is t_i, then the probability ratio for the likelihood of the mixture to the pure state is:

$$R(t_i) = 1 - w + w\frac{\nu_2}{\nu_1}e^{(\nu_1-\nu_2)t_i}\,, \tag{32}$$

where $0 < w \ll 1$ is the fraction of added species 2 and $\nu_2 < \nu_1$ are the Poisson off rates for the added and background species, respectively. A biochemical model is most readily constructed for the log of the probability ratio. Thus we need accumulate $\log(R)$ in Eq. 32. We therefore propose the approximation:

$$\log(R(t_i)) \sim -c_1 + c_2 \max(t_i - T, 0)\,, \tag{33}$$

where $c_1 \sim w$, $c_2 \sim \nu_1 - \nu_2$, and T is an offset defining when the exponential term in Eq. 32 dominates w. A typical mean square error in approximating $\log(R)$ by Eq. 33 is 1% when t_i is sampled from the Poisson distribution $\nu_1 e^{-\nu_1 t}$. An intuitive sense for Eq. 33 is gained from the curve in Fig. S4: the curve with positive drift has negative contributions from very frequent and typical short binding events, while the long-binding events tend to favor the mixture model. The positive value of the drift is controlled by binding events longer than a certain value – the finite value of T where the green curve crosses zero.

The recursion for the ratio of probabilities that the change point θ occurred prior to the current time vs later given a string of occupancy times $t_1, \ldots, t_i$ is

$$e^{\rho(t_i)} \equiv \frac{P(\theta < t_i)}{P(\theta > t_i)} = \frac{R(t_i)}{1-\lambda}(\lambda + e^{\rho(t_{i-1})})\,, \tag{34}$$

where λ is the assumed Poisson probability for the change point time θ to occur at the i-th event. We can then shift ρ to scale out λ, take the log, and approximate $\log(1 + e^{\rho}) \sim \max(\rho, 0)$. Since the change point is signaled by $\rho \gg 1$ the trajectories that actually lead to a hit are not much affected and

the errors made around $\rho \sim 1$ will not seriously alter the value of $t_i - \theta$ when the call is made. After substituting Eq. 33 we can scale out c_2 by setting $c_1 + \log(1-\lambda) = cc_2$ and $\rho = c_2 y$ to generate our final piece wise linear recursion:

$$y' = -c + \max(t - T, 0) + \max(y, 0)\,. \tag{35}$$

We first compute the false positive rate when the random times are sampled from the background distribution $\nu e^{-\nu t}$ (dropping temporarily the subscript 1) a stationary distribution for y only exists when the average additive term in Eq. 35 is negative, i.e.,

$$-c + e^{-\nu T}/\nu < 0\,. \tag{36}$$

We will work in the limit $c \ll 1$ to allow a continuum approximation, which we show in the end is still 5% accurate for $c = 0.5$. Using the so-called Poisson clumping heuristic of Aldous [5] we can compute the false positive rate from the stationary distribution of y and the average residency time for $y \geq y_0$ given that $y \geq y_0$ at $t = 0$ and $y < y_0$ just prior to t (the definition of a "hit"). In what follows we will measure time in integer units as is natural for the recursion in Eq. 35. The conversion to physical time is just to multiply by $1/\nu$.

Clearly the distribution of y is limited to $y \geq -c$ and the small c limit suggests a continuum approximation for the probability distribution function, PDF(y), where the negative values are lumped into a delta function. The equation for the stationary PDF thus reads:

$$\begin{aligned}
\mathrm{PDF}(y) &= A\delta(y) + P(y), \quad y \geq 0\,; & (37)\\
P(0) &= B\,; & (38)\\
P(y) &= (1 - e^{-\nu T})P(y) + c\,\partial_y P(y) + \\
&\quad e^{-\nu T} A\nu e^{-\nu y} + e^{-\nu T}\int_0^y P(y-t)\nu e^{-\nu t} dt\,. & (39)
\end{aligned}$$

The terms in Eq. 39 are fairly transparent. When $t \leq T$, Eq. 35 is just $y' = -c + y$ with $y \geq 0$ so the first two terms are just the Taylor expansion of the shift $P'(y) = P(y + c)$ with a small correction $\sim ce^{-\nu T}\partial_y P$ omitted. The third term is the weight in the PDF at $y = 0$ boosted up by $t > T$. Note we used a property of the Poisson distribution that shifting the time multiplies the probability. The final convolution accounts for events $t > T$

acting on P. The solution of Eq. 39 is elementary by Laplace transformation, $LP(s) = \int_0^\infty e^{-sy} P(y) dy$

$$LP = \frac{-cB + A\nu e^{-\nu T}/(\nu + s)}{-cs + se^{-\nu T}/(\nu + s)} \,. \tag{40}$$

Both A, B can be determined from the condition $LP(0) = 1$ (n.b. the relation $-cB + Ae^{-\nu T} = 0$ is the balance of the flux into $\delta(y)$ from the drift c with the instances of $t > T$ transferring weight from the δ function to $y > 0$) resulting in,

$$\mathrm{PDF}(y) = \frac{\alpha}{\nu}\delta(y) + \frac{\alpha e^{-\nu T}}{\nu c} e^{-\alpha y} \tag{41}$$

$$\alpha = \nu - e^{-\nu T}/c > 0 \,, \tag{42}$$

(and the sign of α follows from Eq. 36). We have compared Eq. 41 with numerical simulations, and even for $c = 0.5$ (and thus not in the limit $c \ll 1$) the errors in PDF for the weight at $y = 0$ and the exponent α are less than 5%, so the continuum limit is quite acceptable. (A diffusion approximation to Eq. 39 would entail expanding the denominator of Eq. 40 to $O(s^2)$. The result for $P(y)$ would be two exponentials $\sim e^{-\nu y}, e^{-\nu e^{\nu T} c\alpha y}$ that both decay more rapidly than $e^{-\alpha y}$.)

The profile of y vs time is a sawtooth with a uniform decrease of $-c$ per step, punctuated by rare jumps upward with a distribution $\sim e^{-\nu y}$ where y is the value after the jump. To compute Poisson rate for hitting a cutoff y_0 we divide the total probability for $y \geq y_0$ from Eq. 41 with the average dwell time for $y \geq y_0$ given that at the preceding iteration $y < y_0$. In the limit $\nu c \gg e^{-\nu T}$ the dwell time is just $1/(\nu c)$ which represents the average distance above y_0 that y is kicked divided by the amount it decreases per iteration. When the probably of a second kick while y is near y_0 is not negligible a more sophisticated calculation is needed for the dwell time.

Since we work in the limit $e^{-\nu y_0} \sim 0$ with boundary conditions $P(0 \leq y \ll y_0) \sim 0$ we can write the recursion relation for the smooth part of the PDF following Eq. 39 as:

$$P^{'}(y) = (1 - e^{-\nu T})P(y) + c\partial_y P(y) + e^{-\nu T} \int_0^y P(y - t)\nu e^{-\nu t} dt \,. \tag{43}$$

The dwell time τ can then be computed by Laplace transforming and iterating the recursion in Eq. 43. The initial condition $P_0(y)$, must be proportional

to $e^{-\nu y}$ since that is the functional form of the events that will kick y over y_0. To compute the dwell time from the integral over $y > y_0$ of the iterates of Eq. 43, requires that P_0 is zero for $y < y_0$ and is normalized to one. Its Laplace transform is just $LP_0(s) = \frac{\nu}{\nu+s} e^{-sy_0}$. Then we find for the dwell time τ,

$$\tau \equiv \sum_{i=0}^{n-1} \int_{y_0-\epsilon}^{y_1} P_i(y)\,, \tag{44}$$

$$\tau = \int \Big(\frac{e^{(y_1-y_0)s} - y^{-\epsilon s}}{s} \Big) \frac{(e^{n\beta}-1)\nu}{\beta(\nu+s)}\,, \tag{45}$$

$$\beta = cs - \frac{s}{\nu+s} e^{-\nu T}\,. \tag{46}$$

Some care is needed to deform the integration contour for the inverse Laplace transform. The manipulations become clearer if one does not expand the discrete time iteration Eq. 43 for $P(y)$ for small c but rather writes the first two terms as $(1 - e^{-\nu T})P(y + c)$ which is readily Laplace transformable if one assumes that $P(0 \ll y \ll y_0) = 0$ as allowed in Eq. 43 since we are calculating only the dwell time in the limit of large y_0. The real part of the inversion contour can be moved through $s = 0$ with zero residue and the contour closed to the left. The large y_1, n limit can then be taken. There remains a single pole at $-\nu + e^{-\nu T}/c$, which is proportional to the average drift velocity Eq. 36. As expected, the mean dwell time diverges when the mean drift downward in y tends to zero.

Thus,

$$\tau = 1 + \frac{\nu/c}{(\nu - e^{-\nu T}/c)^2} \tag{47}$$

$$\gamma = \int_{y_0}^{\infty} PDF(y)/\tau = \frac{e^{-\alpha y_0}}{\nu c \tau e^{\nu T}}\,, \tag{48}$$

where γ is the Poisson rate for hitting the cutoff y_0 in units of per iteration and a 1 was added to Eq. 47 to account for the ambiguity in adjusting the Poisson jump for c and to avoid nonsense for small τ, though our approximations are only valid for $\tau \gg 1$. Note τ in the limit $e^{-\nu T} \ll c\nu$ agrees with expectations. Numerical simulations give roughly 10% agreement with γ which is in part due to ambiguities in the simulation of deciding when short intervals with $y < y_0$ represent the same or distinct hits.

The entire derivation from Eq. 39 onward can be generalized to t_i sampled from a mixture Q of Poissons. The $e^{-\nu T}$ is replaced by the total probability weight for $t \geq T$ and the appropriate t distribution has to be convoluted with P. The Laplace transform of Eq. 40 is a rational function with Q poles which give a sum of Q terms of the form $e^{-\alpha_q y}$ in Eq. 41. Similar complexities occur in the derivation of τ.

References

[1] Redner S (2001) *A Guide to First-Passage Processes*. Cambridge University Press.

[2] Wald A (1948) *Sequential Analysis*. Dover Publs., New York.

[3] Cover TM, Thomas JA (2006) *Elements of Information Theory*. John Wiley, New York.

[4] Gradshteyn IS, Ryzhik IM (2000) *Table of Integrals, Series and Products*. Sixth Ed., Acad. Press, New York.

[5] Aldous D (1989) *Probability approximations via the Poisson clumping heuristic*. Springer-Verlag, New York.